Resonance Parameters from Lattice QCD

Dehua Guo

May 12, 2015

Physics Department, Columbian College of Arts & Sciences,

George Washington University, DC 20052

A dissertation proposal submitted to
the faculty of
The Columbian College of Arts and Sciences
of The George Washington University
in partial fulfillment of the requirements for the degree of
Doctor of Philosophy

Dissertation proposal directed by
Andrei Alexandru

1 Introduction

We propose to study hadronic scattering using Lattice Quantum Chromodynamics (LQCD). In particular, we will first focus on the mesonic resonances such as $\rho(770)$ in isospin $I = 1$, spin $J = 1$ channel of pion-pion scattering and $K^*(892)$ in $I = \frac{1}{2}$, $J = 1$ channel of kaon-pion scattering. Another direction of interest is the resonances in the baryon-meson scattering such as $N(1440)$ with quantum numbers $I = \frac{1}{2}$ and $J = \frac{1}{2}$. We choose the mesonic scattering as our starting point because in Lattice QCD meson observables have better signal-to-noise ratio than baryonic ones.

The motivation for this study is threefold. First of all, lattice QCD calculations of resonance parameters that are well determined experimentally serve as a test of QCD. Lattice QCD offers us a way to study the resonances starting from first principles, directly in terms of quark and gluon dynamics. Hadron scattering is the main tool to investigate experimentally the strong force and computing phase-shifts will allow us to directly compare the predictions of theory and experiment. Secondly, these studies will serve to validate the methodology that can then be used to investigate systems where the experimental situation is less clear (for example this is currently done for charm hadrons). Thirdly, LQCD can be employed to validate and refine effective models used to describe hadron scattering. These models are mainly tuned using experimental input, but LQCD can provide additional input for systems where quark masses are modified from their physical values.

The plan of the presentation is the following: in the next section, we summarize the relevant features of QCD, the theory that describes the interaction between quarks and gluons. In section 3, we review the status of current lattice QCD investigations of the $\rho(770)$ and $K^*(892)$ resonances and the techniques used. To help us describe the methods we plan to use in our study, we include an introduction to LQCD in Section 4. In Section 5 we will describe the techniques used to extract the energy of the multi-hadron states and discus the connection between the symmetries of the lattice system and the continuum. In Section 6 we present Lüscher's formula which provides the connection between phase-shifts and the energies of multi-hadron states and discuss the extraction of scattering parameters from the phase-shifts. In Section 7 we present our preliminary calculation for the $\rho(770)$ resonance parameters. In Section 9 we present our planned timeline for this study.

2 Quantum Chromodynamics

There are four types of fundamental interactions: gravitational, electromagnetic, strong and weak. All of them are understood as the dynamics of fields. The theory that describes the electromagnetic, strong and weak interactions in subatomic particles is called the Standard Model. This is a theory that combines relativity and quantum mechanics, and describe all observables using a collection of fundamental fields. These fields are the matter fields (quarks and leptons) which are fermionic, and interaction fields (photons, gluons, W and Z bosons) which are bosonic; both electroweak and strong interactions are introduced using gauge theories. There are six leptons and six quarks arranged in three families that are identical in most respects except for their masses. This hints to a further substructure but currently there is no theory that explains this regularity adequately. The dynamics of hadrons is in large part determined by the strong force, with small corrections induced by the electroweak interactions. To a very good approximation the hadrons' spectrum and their interactions can be determined neglecting the electroweak forces and we will do so in this study.

Quantum chromodynamics (QCD) is the generally accepted theory describing the strong interactions between quarks and gluons that make up hadrons. The quarks come in six flavors: up, down, strange,

charm, bottom and top. As far as QCD is concerned, the flavors are identical differing only by mass. The Lagrange density of QCD is

$$\mathscr{L}_{QCD} = -\frac{1}{2}\,\mathrm{Tr}\,F_{\mu\nu}F^{\mu\nu} - \sum_f \bar{\psi}_f \gamma^\mu \left[\partial_\mu - igA_\mu\right] \psi_f - \sum_f m_f \bar{\psi}_f \psi_f, \tag{1}$$

where $F_{\mu\nu} = \partial_\mu A_\nu - \partial_\nu A_\mu + ig[A_\mu, A_\nu]$ is the field strength tensor, $\bar{\psi}_f$ and ψ_f are antiquark and quark fields, A_μ is a gauge field, g is the coupling, m_f is the mass of the quark, and f is the flavor index. In QCD the gauge field A_μ has values in the $su(3)$ Lie algebra associated with the gauge group $SU(3)$. The quark fields transform under the fundamental representation of the group and the gauge field under the adjoint representation. The charge associated with the gauge group is called color and the basis for the three-dimensional fundamental representation is usually labeled using the primary colors (red, blue and green). Due to the non-abelian structure of the gauge group, the force carriers, the eight types of gluons corresponding to the generators of $SU(3)$, are charged and interact directly with one another.

There are only a few parameters in QCD: the gauge coupling constant g and the quark masses m_f for each flavor. Note that the gauge coupling is scale dependent, that is it depends on the energy scale of the experiment used to define the coupling. One important feature of QCD is *asymptotic freedom* - the fact that the coupling constant becomes small at high energies and vanishes in the ultraviolet limit. This leads to approximative scaling in high energy scattering and it also enables the use of perturbative methods to compute cross-sections for energetic collisions. This peculiar behavior of the coupling constant is due to the anti-screening of color charges, which in turn is due to the contribution of gluons to the vacuum polarization.

On the other hand, the coupling constant becomes strong at low energies. Since the coupling is not a physical observable and depends on the energy scale, the overall scale of the theory can be set either by specifying the renormalized coupling at a given energy or by indicating the energy scale where the coupling becomes strong. This latter parameter is denoted by Λ_{QCD} and its value is about 200–300 MeV (the precise value depends on the definition). This is the scale where non-perturbative effects become important. At this scale, the hadronic scale, the interaction becomes very strong and the quarks and gluons become *confined*. Experimentally this is signaled by the lack of colored states: no free quarks or gluons have been observed. All states observed experimentally are color neutral. From a quark model point of view they are either mesons (quark-anti-quark states) or baryons (states with three valence quarks).

Finally, we note that of the six quark flavors, three of them: charm, bottom and top quarks, are too heavy to have a significant effect on the spectrum of light hadrons, and they can be safely neglected.

3 Resonances from Lattice QCD – a review

While the theoretical foundations for studying scattering from Lattice QCD were developed in 1980s, it is only in recent years that significant progress has been made in computing scattering parameters for hadrons. The main reasons behind this are the fact that only recently dynamical lattice QCD simulations can be performed with quark masses close to the physical ones and on box sizes large enough so that resonances such as ρ become unstable and mix with the two-particle states. On another hand, new developments of variational techniques allow the extraction of energies when these states mix, which in turn allows us to compute the scattering phase-shifts accurately. Nevertheless, these calculations are computationally expensive and only a few channels were studied. The first studies focused on mesonic systems mainly because when compared to the baryonic sector the signal-to-noise ratio is better and

the number of quark lines involved is reduced and there are fewer Wick contractions that need to be evaluated. This becomes important when computing a large variational basis, as we will see in latter sections. In this section, we are going to review the lattice QCD studies focused on the $\rho(770)$ and $K^*(892)$ resonances.

3.1 $\rho(770)$ resonance

In this section we review the lattice studies focused on the $I = 1$ channel for $\pi - \pi$ scattering in the ρ resonance region. The results of these studies and the simulation parameters are collected in Table 1. Below we list the salient features of each of these studies.

An early lattice estimate of the $\rho \to \pi\pi$ amplitude [1] did not use Lüscher's method to get the scattering phase shift from the lattice energy spectrum simulation. It studied the decay of a vector meson to two pseudoscalar mesons on rather small lattices with the sea quark mass set to the value of the strange quark mass. In spite of this the study extracted an effective coupling consistent with the experimental value and it performed a number of cross-checks to validate the method used in the paper. However, the method did not seem easily generalizable to other systems and it was largely equivalent with Lüscher's method, so the latter studies did not employ the same technique.

In 2007, S. Aoki et al. [2] performed a LQCD calculation of the ρ meson decay width via the P-wave scattering phase shift for the two-pion system in the moving frame. The study uses full QCD gauge configurations with $N_f = 2$ flavors on a $12^3 \times 24$ lattice. A $\pi\pi$ interpolator and a ρ interpolator were used to construct a 2×2 correlation matrix. The ground state and first excited state energy were extracted using the variational method. A followup study [3, 4] updated their results to $N_f = 2 + 1$ full QCD configurations with pion mass $m_\pi = 410\,\text{MeV}$ and $m_\pi = 300\,\text{MeV}$ on a $32^3 \times 64$ ($L = 2.9\,\text{fm}$) lattice. The $\pi\pi$ correlation functions were evaluated using stochastic source methods. To extract the phase shifts the moving frame method developed by Rummukainen and Gottlieb [5] was used.

A study by X. Feng et al. [6] used $N_f = 2$ configurations and twisted-mass fermions action with $m_\pi = 480\,\text{MeV}$ and $420\,\text{MeV}$ with $L = 1.9\,\text{fm}$, and $m_\pi = 330\,\text{MeV}$ and $290\,\text{MeV}$ with $L = 2.5\,\text{fm}$. This study contains both the center of mass frame (by Lüscher [7]) and the moving frame method which can allow us to compute the scattering phase shift at more energies using the same lattice size and can increase the accuracy of the calculation of the desired resonance parameters for less computational cost. The same 2×2 correlation matrix as above is used for the variational method. This study is notable for using a large set of quark masses, but the results both for ρ mass and for the $g_{\rho\pi\pi}$ coupling are larger than expected.

A study done by M. Göckeler in 2008 [8] computes the mass and width of ρ meson from simulation of $N_f = 2$ favors of dynamical clover fermions at small pion masses $2m_\pi < m_\rho$. They only extract the lowest energy in the channel using smeared sources and did not employ a variational method. The error bars are very large for both $g_{\rho\pi\pi}$ and m_ρ. The same authors also developed a generalization of formalism to S-, P- and D-wave meson and baryon resonances in a nonvanishing momentum frame [9].

C. B. Lang et al. [10] were the first group to use a large variational basis and to study the effect of it on the states extracted. This study used a rather small box so it employed the boosted frame formalism to get to the kinematically interesting region. The parameters for the ensembles used in this study were $m_\pi = 266\,\text{MeV}$, $L = 1.98\,\text{fm}$, and $N_f = 2$ with nHYP clover fermions action. In this work they employ 5 quark-antiquark interpolators with three different levels of smearing and one $\pi\pi$ interpolator. They test whether the resulting two levels are robust against the choice of the interpolators because all the ρ meson resonance study used at most one quark-antiquark and one $\pi\pi$ interpolator which may not be reliable if the third energy level is nearby. They are able to construct this large basis because they use

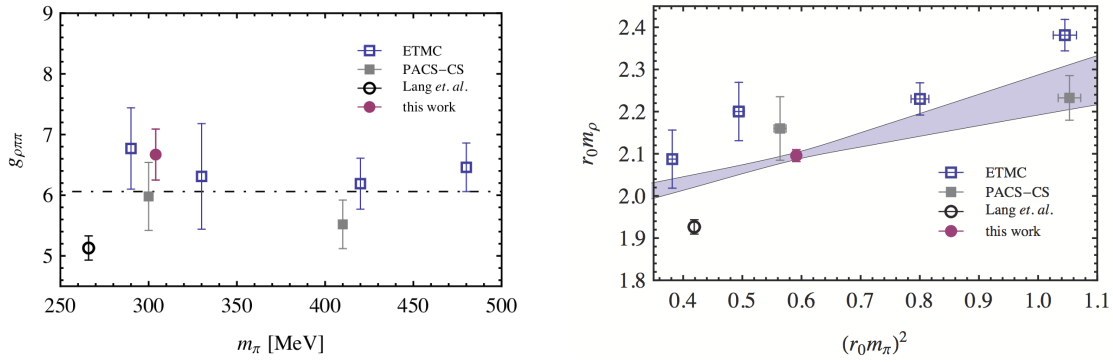

Figure 1: (Left) A comparison of $g_{\rho\pi\pi}$ for several previous studies. (Right) ρ mass as a function of the pion mass. Dimensionless parameters are used so that the error introduced by converting to physical units is eliminated. The band is a result from unitarized χPT based on LQCD data. To convert this data to dimensionless units a value of $r_0 = 0.5\,\text{fm}$ has been used [14].

Laplacian Heaviside (LapH) smearing method [11].

X. Li, C. Liu, and X. Feng [12, 13] generalized the Lüscher's method [7] for two-particle energy eigenstates in an asymmetric rectangular box with periodic boundary conditions in all three directions. This setup was used in a recent study by Alexandru and Pelissier [14] which used nHYP-Clover fermions action with $m_\pi = 300\,\text{MeV}$ and $V = 24^2 \times \eta 24 \times 48$, $L = 3\,\text{fm}$ lattice for η=1.0,1.25, and 2.0. Gauge configurations were generated using the method described in [15]. A 2×2 correlation matrix was employed to extract the ground state and the first excited states. The $\pi\pi$ correlation functions were evaluated using stochastic source methods.

Another recent study by J. Dudek et al. [16] in 2012 use a very large basis of interpolators and extract the phase shifts using three different lattice volumes and many different boosts. This allows them to extract phase-shift for many different energies and they map the resonance region in great detail. They study the effect of two kinds of interpolators both "single hadron" and "multi-hadron" ones. The quark mass used in this study is rather heavy, $m_\pi \approx 390\,\text{MeV}$, and in spite of the large basis used the errors on the extracted parameters is comparable with the ones extracted in the study by

Author (Year)	Fermion action	N_f	m_π (MeV)	L (fm)	a (fm)	m_ρ (MeV)	$g_{\rho\pi\pi}$
Feng (11)	Twisted mass	2	480	1.9	0.079	1118(14)	6.46 (40)
Feng (11)	Twisted mass	2	420	1.9	0.079	1047(15)	6.19 (42)
Feng (11)	Twisted mass	2	330	2.5	0.079	1033(31)	6.31 (87)
Feng (11)	Twisted mass	2	290	2.5	0.079	980 (31)	6.77 (67)
Aoki (11)	Wilson	$2+1$	410	2.9	0.091	893 (13)	5.52 (40)
Aoki (11)	Wilson	$2+1$	300	2.9	0.091	863 (27)	5.98 (56)
Lang (11)	nHYP Clover	2	266	1.98	0.124	772 (10)	5.61 (12)
Pellisier (12)	nHYP Clover	2	304	3.0	0.125	827 (6)	6.67 (42)
Dudek (12)	Clover	$2+1$	391	1.9–2.9	0.12	854.1(13)	5.80 (10)

Table 1: ρ resonance decay parameters results from various studies. The experimental value for ρ resonance are $m_\rho = 775.49(34)\,\text{MeV}$, $\Gamma_\rho = 149.1(8)\,\text{MeV}$.

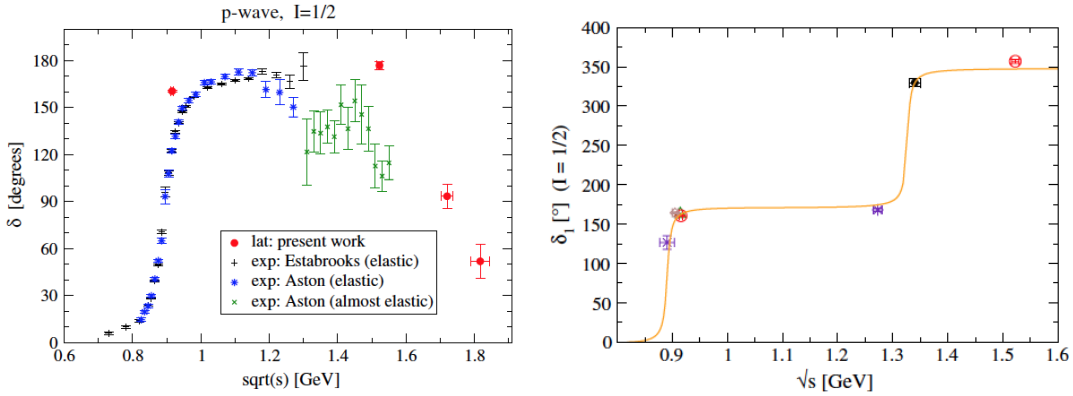

Figure 2: Phase shift in $I = 1/2$ p-wave channel. Figures from C. B. Lang et al. [18] (left) and S. Prelovesek et al. [19] (right). Only one lattice simulation data point is closed to the resonance region. $\sqrt{s} \approx 0.89$ GeV.

C. B. Lang et al [10]. They also use LapH to help them construct the operatorial basis.

The results from some of these studies are summarized in Fig. 1 which is taken from [14]. We can see that the coupling constant $g_{\rho\pi\pi}$ is relatively stable around 6 for all quark masses. However, the result from Lang et al. [17] has a $g_{\rho\pi\pi}$ around 5 with a small errorbars. As it turns out this was due to an error in their code. After fixing their error, their results $g_{\rho\pi\pi} = 5.61(12)$ is closer to the value in the physical limit. In any case the currently available data is not precise enough to allow for a tight extrapolation to the physical point. The first project we plan to work on will provide this input, as we will see in Section 7.

3.2 $K^*(892)$ resonance

$K\pi$ scattering is the simplest reaction that includes a s quark and direct lattice QCD measurement of $I = 1/2, 3/2$ channel will provide a test of the validity of chiral perturbation theory for $N_f = 2+1$ system. Like $\rho(770)$, the $K^*(892)$ resonance also has the angular momentum $J = 1$. Hence, the study of K^* requires only a minimal extension of the methods used in studying the ρ resonance. It is important to note that the kinematics of the collision change and most likely we will need different lattice geometries and boost. Furthermore, the lack of symmetry compared to $\pi\pi$ scattering, introduces a mixing of the channels with different quantum numbers and additional effort is required to disentangle the channel of interest. Recently a few of studies focused on $K\pi$ scattering on the lattice. They studied all combinations of $I = 1/2$, and $I = 3/2$, and s-wave($l = 0$) and p-wave($l = 1$) channels. However, there are still relatively few data points in K^* resonance region.

In C. B. Lang et al. [18], $K\pi$ scattering is studied in all four channels: $I = 1/2$, $I = 3/2$ and $l = 0$, $l = 1$. The authors use only states with total momentum $\boldsymbol{P} = 0$ to avoid the mixing between the s-wave and p-wave channels. In $I = 1/2, l = 1$ channel which corresponds to the resonance $K^*(892)$ that we are interested in, the authors are only able to extract one phase shift near $\sqrt{s} \approx m_{K^*}$ as can be seen from left panel of Fig. 2. Assuming that the coupling is the same as in the physical case, the width of the resonance for their pion mass is reduced to 14 MeV. Using this value of the width, their single phase-shift predicts that the resonance has a mass of 896 MeV.

A Lattice QCD study of $K^*(892)$ resonance using states with non-zero total momentum was carried out by Z. Fu and K. Fu [20]. They use $N_f = 2+1$ gauge configuration with asqtad improved staggered

quarks. They extract two phase-shift values using a stochastic source method and attempt to fit these values using a Breit-Wigner form. The value of the coupling and resonance mass depend strongly on whether a continuum form for the dispersion relation is used or a lattice version. This may be due to the rather coarse lattice spacing used in this study, $a = 0.15\,\text{fm}$. The results are in broad agreement with experiment, but the results are still quite preliminary.

In 2013, S. Prelovesek et al. [19] did a followup study to C. B. Lang et al. [18], where they also used non-zero total momentum states. This allows them to extract the phase-shifts for more than one energy, but most of the data seems to be away from the resonance region, as can be seen from the right panel of Fig. 2. They fit the data to a Breit-Wigner form and extract a mass for the resonance and coupling in good agreement with the experimental result. The error bars are very large, at least for the coupling, and given the fact that the phase-shifts are only defined up to a multiple of 180° it is unclear how reliable their extraction of the resonance mass is.

To sum up, the studies for this resonance are quite preliminary and more data points are required to pin down the mass and width of this resonance and to study its dependence on quark masses.

4 Lattice QCD

The basic tool for studying strong interaction dynamics of hadrons is the scattering experiment. The observable measured is the scattering cross-section which quantifies the strength of the interaction between particles. The angular dependence of the cross-section can be used to decompose this into partial waves and extract phase-shifts as a function of the center-of-mass energy in different channels. Unfortunately, Lattice QCD cannot directly compute the scattering amplitude since the infinite-volume Euclidean space Green's functions are not directly related to two or more particles scattering except at kinematic thresholds. This is known as "Maiani-Testa no-go theorem" [21]. A solution derived by Martin Lüscher [7] uses a connection between finite-volume two-particle energies in a periodic box and the phase-shifts for elastic scattering to overcome this limitation. This method was later extended to states with non-zero total momentum and asymmetric boxes. In this section we will discuss the formulation of QCD on a lattice and in the next section we will show how to compute energies for single- and multi-hadron states using lattice QCD.

Before lattice formulations of QCD by Kenneth Wilson in 1974, all predictions of QCD were restricted to the pertubative energy regime. The lattice formulation allows us to study QCD non-perturbatively using numerical methods. In order to discuss QCD in a mathematically well-defined way, LQCD replaces the 4-dimensional continuous space-time by an Euclidean 4-dimensional discrete space-time lattice which naturally introduces a momentum cut-off at the order $1/a$, where a is the lattice spacing. In principle, in the $a \to 0$ limit, the continuum QCD is recovered. Numerical simulations of LQCD are carried out using finite volume boxes with specific boundary conditions and spectral information is extracted using correlation functions.

The review here is minimal, covering only the elements relevant for our calculations. For a detailed description of Lattice QCD the reader is referred the standard textbooks by Rothe [23] and Gattringer and Lang [22], which were the inspiration for the material in this section.

The starting point of LQCD formulation is the Euclidean path integral. In Euclidean framework, which formally corresponds to a rotation to imaginary time $t \to -ix_4$, a quantum mechanical theory becomes equivalent to a statistical mechanics problem. Physical observables can be computed by using statistical method with a space-time lattice. All the information is encoded in n-point functions. For

example, spectral information is extracted from two point functions:

$$\left\langle O_2(t)O_1^\dagger(0)\right\rangle = \frac{1}{Z}\int D[\psi,\bar{\psi},A]e^{-S_{QCD}[\psi,\bar{\psi},A]}O_2[\psi_t,\bar{\psi}_t,A_t]O_1^\dagger[\psi_0,\bar{\psi}_0,A_0]\,, \tag{2}$$

where ψ and $\bar{\psi}$ are fermionic fields, A is the gauge field, O_1 and O_2 are interpolators which are chosen to have the desired overlap with the states we are interested in. The normalization factor Z, also called the partition function by analogy with statistical mechanics, is:

$$Z = \int D[\psi,\bar{\psi},A]e^{-S_{QCD}[\psi,\bar{\psi},A]}\,. \tag{3}$$

The QCD action is a sum of the gluonic and fermionic contributions: $S_{QCD} = S_G + S_F$. We will discuss the lattice discretization for each of these parts next.

4.1 Lattice discretization

The QCD action on the lattice is the discretization action which is non-unique. In this section we will discuss Wilson discretization for the gauge action S_G and for the fermionic fields.

On the lattice the fermionic fields are sampled at the grid points and the gauge field is introduced as using the parallel transporters between adjacent sites. These transporters are elements of the gauge group $SU(3)$ rather than the associated algebra, as is the case in the continuum. We denote these transporters with $U_\mu(n)$ with a directional index μ which is attached to the link between the points n and $n+\hat{\mu}$ pointing in the $\hat{\mu}$ direction. Under a gauge transformation the gauge field changes as

$$U_\mu(n) \to U'_\mu(n) = \Omega(n)U_\mu(n)\Omega(n+\hat{\mu})^\dagger, \tag{4}$$

where $\Omega(n)$ is the gauge transformation at site n.

The Wilson gauge action can be written as:

$$S_G[U] = \frac{2}{g^2}\sum_n\sum_{\mu<\nu}\text{Re tr}\left[\mathbf{1}-U_{\mu\nu}(n)\right]\,, \tag{5}$$

where $U_{\mu\nu}(n)$ is the shortest non-trivial closed loop called the *plaquette*:

$$U_{\mu\nu}(n) = U_\mu(n)U_\nu(n+\hat{\mu})U_{-\mu}(n+\hat{\mu}+\hat{\nu})U_{-\nu}(n+\hat{\nu})\,. \tag{6}$$

One can show that for a smooth field A_μ, if we use

$$U_\mu = \exp\left(ig\int_n^{n+\hat{\mu}}A_\mu dx_\mu\right)\,, \tag{7}$$

when the lattice size $a\to 0$, then $\lim_{a\to 0}S_G^{\text{lat}}[U] = S_G^{\text{cont}}[A]$, that is, Wilson gauge action matches the continuum action as it approaches the continuum limit.

For the fermionic part of the action S_F, we start from the "naive" finite-difference discretization of the fermionic action:

$$S_F[\psi,\bar{\psi},U] = a^4\sum_f\sum_n\bar{\psi}_f(n)\left(\sum_{\mu=1}^4\gamma_\mu\frac{U_\mu(n)\psi_f(n+\hat{\mu})-U_{-\mu}(n)\psi_f(n-\hat{\mu})}{2a}+m_f\psi_f(n)\right). \tag{8}$$

We can see that the fermionic action is bilinear in ψ and $\bar{\psi}$, it can be written as:

$$S_F[\psi,\bar{\psi},U] = a^4 \sum_f \sum_{n,m} \sum_{a,\alpha,b,\beta} \bar{\psi}(n)^a_{f\alpha} D_f(n|m)^{ab}_{\alpha\beta} \psi(m)^b_{f\beta}, \tag{9}$$

where $D_f(n|m)^{ab}_{\alpha\beta}$ is the lattice Dirac operator in terms of the gauge field, f is the flavor index, a and b are color indices, α and β are spinorial indices, and n,m are site positions.

However, there is a problem with this "naive" discretization. To see this, we look at the momentum space expression for free field, that is when gauge fields $U_\mu(n) = \mathbf{1}$:

$$\tilde{D}_f(p) = m_f \mathbf{1} + \frac{i}{a} \sum_{\mu=1}^{4} \gamma_\mu \sin(p_\mu a). \tag{10}$$

The lattice operator above has the expected behavior of $m_f + \gamma_\mu p_\mu$ when $p \approx 0$, but it has additional unphysical poles at the points where $\gamma_\mu \sin p_\mu = 0$:

$$p = (\pi/a,0,0,0),(0,\pi/a,0,0)... \tag{11}$$

which do not exist in continuum case. These leads to the appearance of spurious quark flavors in the lattice formulation called doublers. This is called the fermion doubling problem. To remove the doublers Wilson suggested to add a term to the lattice Dirac operator

$$\tilde{D}_f(p) = m_f \mathbf{1} + \frac{i}{a} \sum_{\mu=1}^{4} \gamma_\mu \sin(p_\mu a) + \mathbf{1} \frac{1}{a} \sum_{\mu=1}^{4} (1 - \cos(p_\mu a)). \tag{12}$$

This term acts like an additional mass term and the mass of the doublers is $m_f + \frac{2l}{a}$ where l is the number of non-zero components in the momentum p at the position of the associated pole. In the limit $a \to 0$ the doublers become very heavy and decouple from the fermionic action.

In the position space the Wilson Dirac operator has the form

$$D_f(n|m)^{ab}_{\alpha\beta} = \left(m_f + \frac{4}{a}\right) \delta_{\alpha\beta} \delta_{ab} \delta_{nm} - \frac{1}{2a} \sum_{\mu=\pm1}^{\pm4} \left(\mathbf{1} - \gamma_\mu\right)_{\alpha\beta} U_\mu(n)_{ab} \delta_{n+\hat{\mu},m}, \tag{13}$$

where $\gamma_{-\mu} = -\gamma_\mu, \mu = 1,2,3,4$.

For our simulations we use an improved discretization for both gauge and fermionic actions. They differ from the discretizations presented above by *irrelevant* terms, terms that vanish in the continuum limit. These terms are added to make the approach to the continuum faster.

4.2 Numerical aspects

Since the fermionic action is a bilinear in the $\bar{\psi}$ and ψ fields, it can be integrated out analytically using Grassmann algebra:

$$Z_F[U] \equiv \int D[\psi,\bar{\psi}] e^{-S_F[\psi,\bar{\psi},U]} = \int D[\psi,\bar{\psi}] \exp\left(-\sum_f \bar{\psi}_f D_f[U] \psi_f\right) = \prod_f \det D_f[U], \tag{14}$$

where we made the dependence on the gauge field U explicit. The correlation functions can then be expressed as integrals over the gauge field configurations:

$$\langle O \rangle = \frac{1}{Z} \int D[U] e^{-S_G[U]} Z_F[U] \langle O \rangle_F [U], \tag{15}$$

where $\langle O \rangle_F [U]$ is the fermionic average of the observable:

$$\langle O \rangle_F [U] = \frac{1}{Z_F} \int D[\psi, \bar{\psi}] e^{-S_F[\psi\bar{\psi},U]} O[\psi, \bar{\psi}, U] . \tag{16}$$

For observables that depend on the gauge field alone $\langle O \rangle_F = O$, but when the observables depend on the fermionic field, as is the case for hadron interpolating functions, these averages lead to Wick contractions.

The integral over the gauge fields in Eq. 15 can be evaluated numerically using Monte-Carlo methods by treating it as an average over configurations U with the probability measure

$$P[U] = \frac{1}{Z} e^{-S_G[U]} \prod_f \det D_f[U] , \tag{17}$$

when this measure is positive definite, as is the case for these types of simulations.

To calculate the averages, we use importance sampling technique to generate N gauge configurations distributed with the measure $P[U]$ and then evaluate the observable on each configuration. The average is estimated using

$$\langle O \rangle \approx \frac{1}{N} \sum_{n=1}^{N} O[U_n] , \tag{18}$$

which becomes exact in the limit $N \to \infty$. In practice, several hundred gauge configurations are enough to estimate these averages with percent level accuracy.

5 Hadron spectroscopy

The role of Lattice QCD in this proposal is to compute the energies for single and multi hadron states. In the last section we showed how to evaluate numerically two point correlation functions using path integral methods. In this section we will discuss how to use these correlation functions to compute spectral information. We will then review the variational method, a technique that uses information from a collection of correlation functions to extract energies for situations when the eigenstates are nearly degenerate as is the case when two particle states are mixing in the resonance region. Finally, we will discuss the lattice symmetries and how they connect to the continuum ones. This is required to build interpolators that overlap well with the states with quantum numbers of interest.

5.1 Spectral information from correlation functions

To show how spectral information is encoded in the correlators, we need to connect the path integral representation to the operatorial representation. For a two point function we have [23, 22]

$$C(t_2, t_1) \equiv \left\langle O_2(t_2) O_1^\dagger(t_1) \right\rangle = \left\langle 0 \left| \mathscr{T} \hat{O}_2(t_2) \hat{O}_1^\dagger(t_1) \right| 0 \right\rangle / \left\langle 0 \left| 0 \right\rangle \right. , \tag{19}$$

where $\hat{O}_{1,2}$ are the operators corresponding to the interpolors $O_{1,2}$, $\mathscr{T}$ is the time-ordering product, and $|0\rangle$ is the vacuum state. In Lattice QCD we usually evaluate these correlation functions using boxes with finite time extent. Due to time translation invariance $C(t_2, t_1)$ depends only on $t = t_2 - t_1$ and for $t > 0$ we have:

$$C(t)_T \equiv \left\langle O_2(t) O_1^\dagger(0) \right\rangle_T = \frac{1}{Z_T} \mathrm{Tr} \left[e^{-(T-t)\hat{H}} \hat{O}_2 e^{-t\hat{H}} \hat{O}_1^\dagger \right] , \tag{20}$$

where T is the extent in the time direction, H is the Hamiltonian of the system, the operators are now expressed in the Schrödinger picture, and $Z_T = \mathrm{Tr}\exp(-T\hat{H})$ is the partition function.

Now we insert a complete set of energy eigenstates $|n\rangle$ between two operators in Eq. 20 the correlator becomes

$$C(t)_T = \sum_{m,n} \langle m|\hat{O}_2|n\rangle \langle n|\hat{O}_1^\dagger|m\rangle e^{-E_n t} e^{-E_m(T-t)}. \tag{21}$$

When we take the limit $T \to \infty$ we get

$$\lim_{T\to\infty} C(t)_T = \langle 0|\hat{O}_2|1\rangle \langle 1|\hat{O}_1^\dagger|0\rangle e^{-E_1 t}\left(1 + O\left(e^{-\Delta E t}\right)\right), \tag{22}$$

assuming that the vacuum energy $E_0 = 0$ and that either $\langle 0|\hat{O}_{1,2}|0\rangle$ is zero. The speed of convergence depends on $\Delta E = E_2 - E_1$ the energy difference between the first excited state and the lowest state excited by $\hat{O}_{1,2}$. We note here that in principle all possible eigenstates $|n\rangle$ are present, but we can focus on certain channels by choosing interpolators with definite symmetries. We will return to this topic latter.

In practice we cannot take the $T \to \infty$ limit, but we can check whether we are in the regime described by Eq. 22 by plotting the *effective mass*. This is the discrete derivative of the logarithm of the correlator:

$$m_{\text{eff}}(t) \equiv \ln \frac{C(t)}{C(t+1)}. \tag{23}$$

Once the correlator $C(t)$ is dominated by the ground state energy, m_{eff} becomes constant and the plot plateaus at $m_{\text{eff}} = E_1$.

5.2 Variational Method

In principle, we can extract any number of energy levels using multiple exponential fitting form as in Eq. 21 given enough data points. However, this is impractical especially when the energy levels are nearly degenerate, as is the case near the resonance region. To solve this problem, Lüscher and Wolff [24] developed the variational method. The idea is that instead of considering only a single correlator, we construct a $N \times N$ matrix of cross correlators

$$C_{ij}(t) \equiv \left\langle O_i(t) O_j^\dagger(0)\right\rangle, \tag{24}$$

using a set of N interpolators O_i, $i = 1,\ldots,N$, all with the quantum numbers of the resonance we are interested in. Lüscher and Wolff showed that the eigenvalues of $\lambda^{(k)}(t)$ of the correlation matrix $C(t)$ behave as

$$\lambda_k(t \to \infty) = c_k e^{-E_k t}\left(1 + O(e^{-\Delta E_k t})\right), \tag{25}$$

where ΔE_k is the distance of E_k to the nearby energy levels. A more precise bound can be proven for the generalized eigenvalue equation [25]

$$C(t_0)^{-\frac{1}{2}} C(t) C(t_0)^{-\frac{1}{2}} \mathbf{v}_k = \lambda_k(t)\mathbf{v}_k. \tag{26}$$

The eigenvalue $\lambda_k(t)$ behaves as in Eq. 25 but for $t \in [t_0, 2t_0]$ the correction term vanishes at a rate $\Delta E_k = E_{N+1} - E_k$ which is larger than the interlevel separation $E_{k+1} - E_k$. This also shows that the precision of the eigenvalues improves as the number of basis interpolators is increased.

5.3 Lattice symmetries

As we mentioned earlier, a generic interpolator couples the vacuum with all possible states and this would make the extraction of energies from lattice QCD an impossible task. However, if we construct interpolators that transform according to a particular irreducible representation (irrep) of the lattice symmetry group, then we can guarantee that $\langle 0 | \hat{O} | n \rangle = 0$ unless the state $|n\rangle$ also transform under the same representation. The labels of the irrep are the quantum numbers associated with the states $|n\rangle$. The exact cancellations happen only when you consider exact symmetries of the theory, so for a lattice regularized theory we have to consider the symmetries of the lattice.

For the internal symmetries like flavor and isospin, the lattice theory has the same symmetries as in the continuum. For translation when using periodic boundary conditions the symmetry is reduced to a discrete group which leads to a compact space for the momentum. The finite extent of the lattice introduces a discretization of the momentum in this compact space. In any case, the remaining translational symmetry is sufficient to define states with definite momentum. The only significant problem arises with the rotations. In infinite volume the Hamiltonian is invariant under arbitrary spatial rotation $SO(3)$, however, this is no longer true in a finite volume with periodic boundary conditions. In particular, any rotation allowed on the lattice must preserve the periodicity i.e.

$$\psi(R^{-1}x) = \psi(R^{-1}(x + \mathbf{n}L)), \tag{27}$$

where L is the lattice size, $\mathbf{n} \in Z^3$. This leads to additional constrains for the spatial rotation matrix

$$\sum_i R^{-1}_{ji} L_i n_i = m_j L_j \quad m_i \in L. \tag{28}$$

Therefore, the rotational symmetry is reduced from $SO(3)$ to its subgroup O_h if the lattice is cubic and D_{4h} if the lattice is elongated in one direction. As a consequence of the reduction of rotational symmetry, the eigenfunctions can no longer be classified by a single angular momentum value ℓ, in other words, a complete set of quantum numbers on the lattice is not necessarily the same as in the continuum theory. In order to construct the interpolators with right symmetry it is important to understand the relation of the irreps of $SO(3)$ and cubic (or dihedral) irreps. For the cubic group, the irreps and their properties are listed in Appendix A.

In general irreducible representations of $SO(3)$ will become reducible when considering only a subgroup of transformations. It is possible to work out the decomposition of each $2\ell+1$ dimension

cubic group (O_h)		tetragonal group (D_{4h})	
irrep	ℓ	irrep	ℓ
A_1	0,4,6, ...	A_1	0,2,3, ...
A_2	3,6, ...	A_2	1,3,4, ...
F_1	1,3,4,5,6, ...	B_1	2,3,4, ...
F_2	2,3,4,5,6, ...	B_2	2,3,4, ...
E	2,4,5,6, ...	E	1,2,3,4, ...

ℓ	D_{4h}
0	A_1^+
1	$A_2^- \oplus E^-$
2	$A_1^+ \oplus B_1^+ \oplus B_2^+ \oplus E^+$
3	$A_2^- \oplus B_1^- \oplus B_2^- \oplus 2E^-$
4	$2A_1^+ \oplus A_2^+ \oplus B_1^+ \oplus B_2^+ \oplus 2E^+$

Table 2: Left: Angular momentum mixing among the irreducible representations of the octahedral and tetragonal groups. Right: Decomposition of $SO(3)$ irreps into D_{4h} irreps.

subspace for angular momentum ℓ into lattice irreps. Such a decomposition is illustrated in the right panel of Table 2. Since we are building interpolators based on lattice irreps, it is important to collect all continuum irreps that have an overlap with a given lattice irrep. For the cubic and dihedral group this is done in the left panel of Table 2.

For example, when we study $\ell = 1$ angular momentum state on a cubic lattice, we need to construct our interpolators in the three dimensional irrep F_1. The interpolators in this irrep will also mix with $\ell = 3,4,5,6,...$ states. Fortunately, the states with larger ℓ are higher in the spectrum and we can usually safely neglect this mixing.

6 Scattering Observables

To compute the resonance parameters we need to convert the energy spectrum extracted from Lattice QCD to phase-shifts and then fit the phase-shifts in the resonance region to determine the mass and the width of the resonance. In this section we discuss first Lüscher formula that provides the connection between the spectrum and phase-shifts and then Breit-Wigner parameterization of the phase-shift in the resonance region.

6.1 Lüscher formula

As we mentioned earlier, Lattice QCD cannot be used to extract scattering information directly due to the fact that the theory is formulated in Euclidean time [21]. Lüscher showed that a connection can be established between the two-particle spectrum in a finite-box with periodic boundary conditions and the phase-shifts [7]. A detailed derivation of this relation is presented in Appendix B. Here, we show how to apply Lüscher formula to a specific case: the $\rho(770)$ resonance at rest.

In an elongated box, the symmetry group is D_{4h} which has 5 irreducible representations A_1,A_2, B_1, B_2, E. The ρ resonance has quantum number $I = 1$, $J^P = 1^-$. The $J = 1$ representation splits into two irreducible representation $A_2^- \oplus E^-$. We assume that the contribution from angular momentum $\ell \geq 3$ are negligible in the A_2^- channel. This is a good approximation because at small momentum the scattering phase-shift behaves as $\tan\delta_\ell(k) \propto k^{2\ell+1}$. Using the notation from Appendix B, Lüscher's formula for an elongated box becomes

$$\det[e^{2i\delta} - U(\Gamma)] = 0, \text{where } U(\Gamma) = (\mathscr{M}(\Gamma) + i)/(\mathscr{M}(\Gamma) - i) \tag{29}$$

or in a simpler notation

$$\det[\cot\delta - \mathscr{M}(\Gamma)] = 0. \tag{30}$$

If we neglect the contribution from states with $\ell \geq 3$, the A_2^- sectors only overlaps with $\ell = 1$. Hence, matrix $\mathscr{M}(A_2^-)$ is a one dimensional matrix. The matrix element $\mathscr{M}(A_2^-)_{11,11}$ was worked out in [13]. For a lattice with geometry $L \times L \times \eta L$ we have

$$\cot\delta_1 = \mathscr{M}_{11,11} = \mathscr{W}_{00} + \frac{2}{\sqrt{5}}\mathscr{W}_{20}, \tag{31}$$

where

$$\mathscr{W}_{lm}(1,q^2;\eta) = \frac{\mathscr{Z}_{lm}(1,q^2;\eta)}{\pi^{3/2}\eta q^{l+1}}. \tag{32}$$

The $\mathscr{Z}$ function is defined as

$$\mathscr{Z}_{lm}(s,q^2,\eta) = \sum_{\mathbf{n}\in Z^3} \frac{\mathscr{Y}(\tilde{\mathbf{n}})}{(\tilde{\mathbf{n}}^2 - q^2)^s} \tag{33}$$

where $\tilde{\mathbf{n}} = (n_1, n_2, n_3/\eta)$ and $\mathscr{Y}_{lm}(\tilde{\mathbf{n}})$ are the harmonic polynomials

$$\mathscr{Y}_{lm}(\tilde{\mathbf{n}}) = \tilde{n}^l Y_{lm}(\Omega_{\tilde{\mathbf{n}}})\,. \tag{34}$$

The reduced momentum q is determined by the total center of mass energy E of the scattering system

$$q = \frac{kL}{2\pi}, \qquad E = 2\sqrt{m_\pi^2 + k^2}. \tag{35}$$

The strategy is then to extract as many energy levels E_i as possible in the A_2^- channel, for each E_i compute q_i and plug them in the formulas above to determine $\delta(E_i)$. Each energy level will produce a phase-shift. Unfortunately these energy levels are too far apart to scan the resonance region with enough detail. To scan finely through the resonance we use a number of ensembles with different elongations.

6.2 Resonance parameterisation

The resonances of interest in our study, $\rho(770)$ and $K^*(892)$, are reasonable narrow and are well described by a Breit-Wigner form. The relativistic Breit-Wigner parametrization for the scattering amplitude A_l for two-particle scattering resonances in the center-of-mass frame is

$$A_l = \frac{-E\Gamma_l(E)}{E^2 - M_R^2 + iE\Gamma_{\text{tot}}(E)}, \tag{36}$$

where E is the center-of-mass frame energy, M_R is the mass of the resonance, Γ_{tot} is the full width at half maximum height of the resonance (decay rate), and Γ_l is the l^{th} partial wave decay rate. The relation between scattering amplitude and phase shift for the p-wave in the resonance region is

$$A_1 = e^{i\delta_1(E)} \sin\delta_1(E). \tag{37}$$

Combining the two equations above for p-wave we get

$$\cot(\delta_1(E)) = \frac{M_R^2 - E^2}{E\Gamma_r(E)}\,. \tag{38}$$

The decay width Γ_R is equal to the decay rate function $\Gamma(E)$ at the resonance

$$\Gamma_R = \Gamma_r(M_R). \tag{39}$$

The width of a resonance depends on the phase space available for the decay, which changes significantly when the quark mass changes. This makes it difficult to compare the lattice results with the physical ones. A more useful parametrization is in terms of a coupling constant, which is expected to vary mildly as the quark mass changes. The relation between this coupling constant and resonance width is [27]:

$$\Gamma_r(E) \equiv \frac{g_{R12}^2}{6\pi}\frac{p^3}{E^2}, \tag{40}$$

with

$$p = \frac{1}{2E}\sqrt{[E^2-(m_1-m_2)^2]\,[E^2-(m_1+m_2)^2]}. \tag{41}$$

For $\rho \to \pi\pi$ scattering, the center-of-mass momentum becomes

$$p = \sqrt{\frac{E^2}{4}-m_\pi^2}, \tag{42}$$

which gives us the phase-shift

$$\cot(\delta_1(E)) = \frac{6\pi}{g_{\rho\pi\pi}^2}\frac{E(m_\rho^2-E^2)}{(E^2/4-m_\pi^2)^{3/2}}. \tag{43}$$

For $K^* \to K\pi$ scattering, we have

$$p = \frac{1}{2E}\sqrt{[E^2-(m_K-m_\pi)^2]\,[E^2-(m_K+m_\pi)^2]}, \tag{44}$$

which gives us

$$\cot(\delta_1(E)) = \frac{6\pi}{g_{K^*K\pi}^2}\frac{E(m_{K^*}^2-E^2)}{p^3}. \tag{45}$$

We compute E and m_π using LQCD, and determine $\delta_1(E)$ using Lüscher's method for both $\rho \to \pi\pi$ and $K^* \to K\pi$ scattering. Once we have those results, we can fit Eq. 43 and Eq. 45 to determine $g_{\rho\pi\pi}$ and m_ρ, and $g_{K^*K\pi}$ and m_{K^*}, respectively. After obtaining the coupling constant g, we can use Eq. 40 to determine the decay widths.

Note that the parameterisation in Eq. 40 continues to grow at large energy in an unrealistic way, which may create problems when trying to fit a large range of energies above the resonance. To solve this problem, we can introduce the so-called centrifugal barriers factors. If we assume that the interaction region is limited to a range R, the dependence of Γ on energy changes to [28]:

$$\Gamma_r(E) = \frac{g^2}{6\pi}\frac{p^3}{E^2}\frac{1+(p_R R)^2}{1+(pR)^2}, \tag{46}$$

where p_R is the scattering momentum at the resonance mass.

7 ρ resonance project – current status

In this section we describe the status of our project to determine the ρ resonance parameters from lattice QCD. As we discussed earlier, the ρ resonance has received a lot of attention recently. We plan to carry out a precision study for this resonance using variational analysis, LapH valence quark smearing and elongated box method at two quark masses, $m_\pi \approx 310\,\text{MeV}$ and $m_\pi \approx 230\,\text{MeV}$, and test our results against predictions from models such as unitarized χPT [30]. We will first review the technical details for our calculation and then present our preliminary results for $m_\pi \approx 310\,\text{MeV}$.

7.1 Technical details

One of the main difficulties in calculation of resonance parameters from Lattice QCD is the evaluation of multi-hadron interpolators. These interpolators need to be included in the variational basis in order to correctly reproduce the spectrum expected in the resonance region. Unfortunately, in contrast to single-hadron correlators, which can be estimated using a single quark propagator, multi-hadron correlators require *all-to-all* propagators, that is propagators originating from every point on the lattice. One possibility is to use stochastic methods to evaluate these propagators. This method was used by Pelissier and Alexandru to extract ρ resonance parameters for the ensembles at $m_\pi \approx 310\,\mathrm{MeV}$ [14]. The downside of this method is that, on one hand the estimates are noisy and more importantly the quark propagator calculation needs to be repeated every time a new interpolator is evaluated. A more flexible method is to use Laplacian Heaviside smearing [11]. The basic idea is to evaluate the quark propagator in low-momentum quark subspace, which corresponds to a smeared propagator in the position space. This only requires the calculation of the quark propagators for the low momentum states. The cost is proportional with the number of states we want to retain. We stress that this is not an approximation, we could in principle evaluate this with a minimal number of low momentum states. However, if the number of vectors is too small, our interpolars will have a poor overlap with the states of interest and the single exponential behavior will only appear for large times, when the signal-to-noise ratio is bad.

To compute the low momentum quark states, we use the eigenvectors of the three dimensional gauge-covariant Laplacian operator:

$$\tilde{\Delta}^{ab}(x,y;U) = \sum_{k=1}^{3} \left\{ \tilde{U}_k^{ab}(x)\delta(y,x+\hat{k}) + \tilde{U}_k^{ba}(y)^*\delta(y,x-\hat{k}) - 2\delta(x,y)\delta^{ab} \right\} \tag{47}$$

where a,b is the color index. The hadron interpolating fields are constructed by replacing the quark and anti-quark fields with their smeared version:

$$\tilde{u}(t) \to S(t)u(t) = \sum_{\lambda_t} |\lambda_t\rangle \langle\lambda_t| u(t) \tag{48}$$

$$\tilde{\bar{u}}(t) \to \bar{u}(t)S(t) = \bar{u}(t)\sum_{\lambda_t} |\lambda_t\rangle \langle\lambda_t| \tag{49}$$

where $|\lambda_t\rangle$ are the eigenvectors of Laplacian operator. The quark propagator projected to the low momentum space is then

$$\tilde{M}(t_f,t_i)_{\lambda,\lambda'} = \langle\lambda| D^{-1}(t_f,t_i) \left|\lambda'\right\rangle , \tag{50}$$

where D is the fermionic matrix from Eq. 13.

ρ	$\rho^\dagger$	$\Gamma_{t_i}^\dagger$	Γ_{t_f}
$\bar{u}(t)\Gamma_{t_f} e^{i\mathbf{p}} d(t)$	$\bar{d}(t)\Gamma_{t_i}^\dagger e^{-i\mathbf{p}} u(t)$	$-\gamma_i$	γ_i
$\bar{u}(t)\Gamma_{t_f} e^{i\mathbf{p}} d(t)$	$\bar{d}(t)\Gamma_{t_i}^\dagger e^{-i\mathbf{p}} u(t)$	$\gamma_4\gamma_i$	$\gamma_4\gamma_i$
$\bar{u}(t)\Gamma_{t_f} \nabla_j e^{i\mathbf{p}} \nabla_j d(t)$	$\bar{d}(t)\Gamma_{t_i}^\dagger \nabla_j^\dagger e^{-i\mathbf{p}} \nabla_j^\dagger u(t)$	$-\gamma_i$	γ_i
$\bar{u}(t)\Gamma_{t_f} \{e^{i\mathbf{p}}, \nabla_i\} d(t)$	$\bar{d}(t)\Gamma_{t_i}^\dagger \{e^{-i\mathbf{p}}, \nabla_i\} u(t)$	$-\frac{1}{2}$	$\frac{1}{2}$

Table 3: Single hadron interpolators: the first two are strictly local, whereas for the last two the quark and anti-quark are created on neighbouring sites.

To get a precise determination of the energy in the A_2^- channel, we use six different interpolators in the variational basis: four single hadron type interpolators listed in Table 3, and two $\pi\pi$ type interpolators, with back-to-back momentum (100) and (110). We have a 6×6 correlation matrix for the variational method instead of 2×2 as in the previous study [14].

The π interpolators are defined as

$$\begin{aligned}\pi^+(\boldsymbol{p},t) &= \bar{d}(t)\gamma_5 e^{i\boldsymbol{p}}u(t)\,,\\ \pi^-(\boldsymbol{p},t) &= \bar{u}(t)\gamma_5 e^{i\boldsymbol{p}}d(t)\,.\end{aligned} \tag{51}$$

The $\pi\pi$ operator can be constructed from the product of two single-pion operators,

$$(\pi\pi)_{\boldsymbol{P},\Lambda,\mu} = \sum_{\boldsymbol{p}_1^*,\boldsymbol{p}_2^*} C(\boldsymbol{P},\Lambda,\mu;\boldsymbol{p}_1;\boldsymbol{p}_2)\pi(\boldsymbol{p}_1)\pi(\boldsymbol{p}_2)\,, \tag{52}$$

where Λ is the irreducible representation we want to study, μ is the row of the Λ, C is the Clebsch-Gordan coefficients which are listed in [29]. The summation over $\boldsymbol{p}_1^*$ and $\boldsymbol{p}_2^*$ runs over all possible momenta generated by the symmetry transformations from $\boldsymbol{p}_1$ and $\boldsymbol{p}_2$. For total momentum $\boldsymbol{P} = (0,0,0), \boldsymbol{p}_1 = (1,0,0), \boldsymbol{p}_2 = (-1,0,0)$ case, the $\pi\pi$ operator is

$$\pi\pi_{100}(\boldsymbol{p}_1,\boldsymbol{p}_2,t) = \frac{1}{\sqrt{2}}[\pi^+(\boldsymbol{p}_1)\pi^-(\boldsymbol{p}_2) - \pi^+(\boldsymbol{p}_2)\pi^-(\boldsymbol{p}_1)]\,. \tag{53}$$

For $\boldsymbol{p}_1 = (1,1,0)$, $\boldsymbol{p}_2 = (-1,-1,0)$ case, we need to sum all the possible $\boldsymbol{p}^*$ momenta generated by symmetry transformations: $\{(1,1,0),(1,0,1),(1,-1,0),(1,0,-1)\}$. The $\pi\pi_{110}$ operator can be written as:

$$\pi\pi_{110} = \frac{1}{2}(\pi\pi(110)+\pi\pi(101)+\pi\pi(1-10)+\pi\pi(10-1)). \tag{54}$$

In sum, the 6×6 correlation matrix can be written as

$$C = \begin{pmatrix} C_{\rho_i\leftarrow\rho_j} & C_{\rho_i\leftarrow\pi\pi(100)} & C_{\rho_i\leftarrow\pi\pi(110)} \\ C_{\pi\pi(100)\leftarrow\rho_j} & C_{\pi\pi(100)\leftarrow\pi\pi(100)} & C_{\pi\pi(100)\leftarrow\pi\pi(110)} \\ C_{\pi\pi(110)\leftarrow\rho_j} & C_{\pi\pi(110)\leftarrow\pi\pi(100)} & C_{\pi\pi(110)\leftarrow\pi\pi(110)} \end{pmatrix}, \tag{55}$$

where $i,j = 1,\ldots,4$ running over the single-hadron interpolating fields. Depending on the interpolators involved, the elements of the matrix C are either two-, three-, or four-point correlation functions:

$C_{\rho_i\leftarrow\rho_j} = -\Big\langle$ 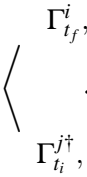 $\Big\rangle$, (56a)

$C_{\rho_i\leftarrow\pi\pi} = \Big\langle$ 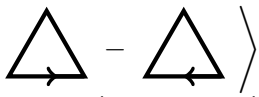 $\Big\rangle \overset{\boldsymbol{P}=0}{=} 2\Big\langle$  $\Big\rangle$, (56b)

$C_{\pi\pi\leftarrow\pi\pi} \overset{\boldsymbol{P}=0}{=} -\Big\langle$ 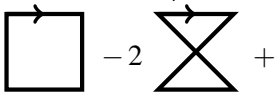 $\Big\rangle$. (56c)

Above the averages are taken over the gauge configurations. The definition of the quark diagrams and the detailed derivation for these correlation functions is included in Appendix C.

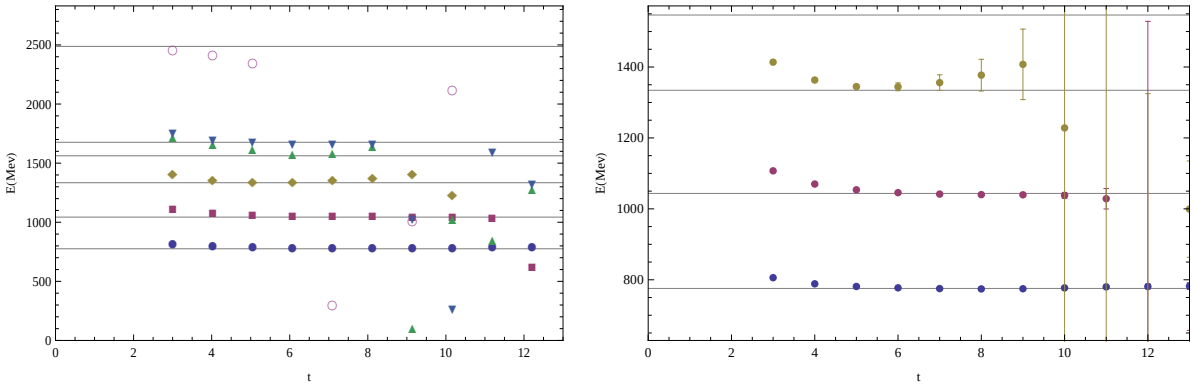

Figure 3: Left: The effective mass for each of the six eigenvalues vs t for the $\eta = 1.0$ ensemble starting from $t_0 = 3$. Right: A closer look at the effective mass for the first three energy eigenstates including their error bars. These are the states used to extract the phase-shifts.

7.2 Preliminary results

In this study, we use three ensembles with different geometries: $\eta 24 \times 24 \times 24 \times 48$, with $\eta = 1.0$, 1.25, and 2.0. We use two mass-degenerate quark flavors with the quark mass tuned such that $m_\pi \approx 310\,\text{MeV}$. Each ensemble has 300 gauge configurations. The lattice spacing for these ensembles is $a = 0.121\,\text{fm}$.

In principle, we should be able to extract as many states as the number of interpolators used in our variational basis. However, as the energy spectrum becomes denser at high energy, the higher energy eigenstates will have larger corrections due to the smaller energy gap between energy levels. To illustrate the quality of our data, the six energy eigenstates for $\eta = 1.0$ ensemble are shown in Fig. 3.

Since we are studying the elastic scattering of two pion with back to back momentum, we will narrow the energy spectrum of two-pion system in the elastic energy region $2m_\pi < E < 4m_\pi$ which for our largest lattice means $750\,\text{MeV} < E < 1370\,\text{MeV}$ (at least two pions have to be in the p-wave). We compute the energy for the lowest three levels (four for the largest lattice) and compute their phase-shifts. The results for the phase-shift together with the Breit-Wigner fits for the standard form (Eq. 38) and the modified form including the barrier terms (Eq. 46) are shown in Fig. 4. The standard form does not fit well the entire energy region unless we restrict only to the points hugging the resonance. On the other hand the Breit-Wigner form with centrifugal barrier terms fits well the data in the entire region. Moreover, the values extracted both for m_ρ and $g_{\rho\pi\pi}$ are almost identical with the ones you get from fitting the standard form to the phase-shift surrounding the resonance.

The values we extract for m_ρ and $g_{\rho\pi\pi}$ are compared with the values from other studies in Fig. 5. We see that our results are in line with the most precise lattice QCD results [10, 16]. Moreover, compared to the earlier calculation by Pelissier and Alexandru (see Fig 1) the new calculation is significantly more precise. This is due to the use of LapH method and the larger interpolating basis. The precise determination of the phase-shifts allows us to discriminate between different parametrizations in the resonance region.

8 Proposed Work

Currently we are finishing up the analysis for the zero momentum states on the $m_\pi \approx 310\,\text{MeV}$ ensembles. We are running the correlation calculation for the same states on the $m_\pi \approx 230\,\text{MeV}$

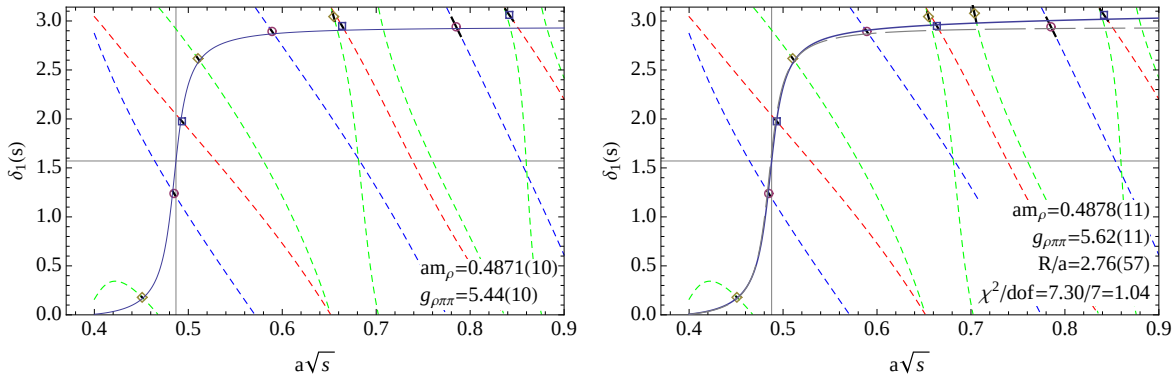

Figure 4: Phase-shifts from three ensembles fitted with Breit-Wigner form (left) and with the modified Breit-Wigner form (right).

ensembles. They are expected to complete soon and we plan to repeat the analysis on these ensembles and extract the resonance parameters for this quark mass. Combining our results with the ones from similar lattice studies, we would like extrapolate the values of m_ρ and $g_{\rho\pi\pi}$ to the physical point and compare it with physical results.

One extension we plan to do is to determine the phase-shifts using for the boosted system for $\pi\pi$ scattering. From Fig. 4, we see that there is only one data point below the resonance energy. Additional points would allow us to better pin down the position of the resonance and the value of the coupling. Moreover, this will allow us to check Lüscher's formula for boosted systems on elongated lattices and whether there is any tension between the zero-momentum data and the ones extracted using the non-zero momentum states. The boosted formalism will be required for the $K\pi$ scattering study in order to access the kinematic region around $K^*(892)$ resonance, so it would be beneficial to check it in the context of $\pi\pi$ scattering where we already have good data.

To study $K\pi$ scattering we need to compute the LapH propagator for the strange quark. We already performed a preliminary study to determine the appropriate mass for the strange quarks. We plan to start production soon for the LapH propagators. While most of the codes will be similar to the ones used for the $\pi\pi$ study, additional quark diagrams will have to be evaluated due to the reduced

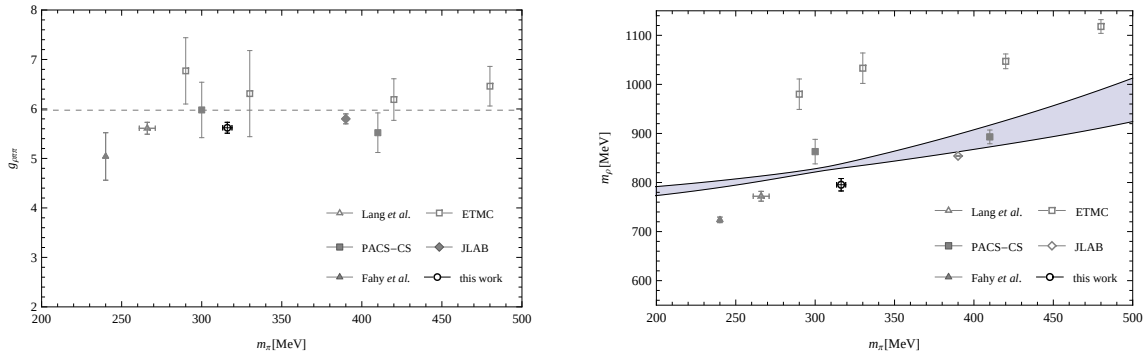

Figure 5: A comparison with results from other lattice groups for $g_{\rho\pi\pi}$ and m_ρ. The dashed line indicates the result at the physical point and the band in the right panel is a unitarized χPT prediction [30].

symmetry. Additionally, the boosted frame formalism for elongated lattices will need to be developed and validated. We hope to be able to generate a few data points in the resonance region and perform an unconstrained fit to extract the mass and width of the resonance. As we discussed in our review in Section 3, all previous results had one or two points in the kinematically relevant region.

While generating the LapH smeared strange quark propagators, we plan to do an exploratory study for nucleon resonance $N(1440)$ in the πN scattering channel. A recent paper [31] focuses on this pion-nucleon system but in the negative parity channel using the boosted frame method. For the positive parity, they find that the excited state in that channel is about 2 GeV, significantly higher than the expected roper resonance. They attribute this failure to an incomplete interpolator basis. The success of this study in the negative parity channel suggests that the signal-to-noise problem is manageable even for meson-baryon systems. Our advantage compared to this study is that we have a set of lattices with different elongations, and we can track the pion-nucleon p-wave state as we vary the relative momentum. The main challenge for this study is deriving the correlation functions for the three-quark nucleon interpolators and the five-quark pion-nucleon interpolators for a suitable set of operators.

9 Research Timeline

The timeline of future research is as follow:

- Complete the computation of LapH quark propagators for three lower pion mass ($m_\pi \approx 230$ MeV) ensembles ($n_x = 24, 28, 32$; $n_y = n_z = 24$; $n_t = 64$) and finish the rest frame ($\mathbf{P} = 0$) analysis by June 2015.
- Extend Lüscher's phase shift formula to boosted frame and finish computing the boosted ($\mathbf{P} \neq \mathbf{0}$) energy spectrum for all ensembles (310 MeV and 230 MeV) by September 2015.
- Write a paper summarizing the study of ρ resonance by September 2015.
- Compute LapH quark propagators for the strange valence quark for all ensembles by November 2015.
- Compute the correlation functions of the nucleon-pion system for all ensembles and analyze the energy spectrum by Spring 2016.
- Finish computing the correlation functions of K^* resonance and obtain the phase-shift pattern and its resonance parameters by December 2016.
- Write thesis and defend by Summer 2017.

Appendices

A Lattice Symmetry group

The special cubic group O_h has 5 irreps which are denoted by A_1, A_2, R, T_1, T_2. The dimensionalities of these representations are 1, 1, 2, 3, and 3. A_1 is the trivial representation and T_1 is the vector representation. The cubic group contains 24 rotations in 5 classes, we label them as:

- E : identity. (1 element)

- C_4^2 : rotations around the three 4-fold axes through an angle of π. (3 elements)
- C_4 : rotations around the three 4-fold axes by $\pm\pi/2$. (6 elements)
- C_2 : rotations around the six 2-fold axes (face diagonals) by π. (6 elements)
- C_3 : rotations around the four 3-fold axes (body diagonals) by $\pm 2\pi/3$. (8 elements)

The characters of the group elements in the five irreps are listed in Table 4. They provide an orthogonal basis which can be used to determine the decomposition of the reducible representations [32]. To determine the decomposition of the $SO(3)$ irreps into O_h irreps, we compute the characters for the O_h group elements in the ℓ irrep of $SO(3)$ (see right panel of Table 4), and then decompose them into the orthogonal basis formed by the characters of the irreps of O_h which are listed in the right panel of Table 4. For example the seven-dimensional irrep $\ell = 3$ has the following components

$$\begin{aligned}
n_{A_1} &= \{7,1,-1,-1,-1\}\cdot\{1,1,1,1,1\}/\|\{1,1,1,1,1\}\|^2 = 0\,,\\
n_{A_2} &= \{7,1,-1,-1,-1\}\cdot\{1,1,1,-1,-1\}/\|\{1,1,1,-1,-1\}\|^2 = 1\,,\\
n_{E} &= \{7,1,-1,-1,-1\}\cdot\{2,-1,2,0,0\}/\|\{2,-1,2,0,0\}\|^2 = 0\,,\\
n_{F_2} &= \{7,1,-1,-1,-1\}\cdot\{3,0,-1,1,-1\}/\|\{3,0,-1,1,-1\}\|^2 = 1\,,\\
n_{F_1} &= \{7,1,-1,-1,-1\}\cdot\{3,0,-1,-1,1\}/\|\{3,0,-1,-1,1\}\|^2 = 1\,.
\end{aligned} \tag{57}$$

Above the scalar product takes into account the multiplicity of each class: $\{1,8,3,6,6\}$. This leads to the decomposition $1 = A_2 \oplus F_2 \oplus F_1$. Similar arguments can be used to derive the decomposition for the dihedral group (see Table 2).

B Lüscher's Formula

To begin, we consider the case of a box with spatial volume

$$V_s = \eta L \times L \times L, \tag{58}$$

where η is real positive number. In $K\pi$ scattering we consider a system of two spinless bosons with different mass m_K and m_π. The states with zero total momentum are described by wave functions $\psi(\mathbf{r})$ satisfying the periodic boundary condition

$$\psi(\mathbf{r}+\mathbf{n}L) = \psi(\mathbf{r}) \text{ for all } \mathbf{n} \in Z^3. \tag{59}$$

Representation	E	C_3	C_4^2	C_2	C_4
A_1	1	1	1	1	1
A_2	1	1	1	-1	-1
E	2	-1	2	0	0
F_2	3	0	-1	1	-1
F_1	3	0	-1	-1	1

ℓ	E	C_3	C_4^2	C_2	C_4
0	1	1	1	1	1
1	3	0	-1	-1	1
2	5	-1	1	1	-1
3	7	1	-1	-1	-1
4	9	0	1	1	1

Table 4: Left: The character table of cubic group with its 5 irreducible representation. Right: The character table for the elements of the cubic group within the ℓ irrep of $SO(3)$.

We can assume that their interaction have a finite range,

$$V(r) = 0 \text{ for } r > R, \tag{60}$$

where r is the spatial distance between two particles. R is called the interaction range.
The Hamiltonian operator is defined by

$$H = -\frac{1}{2\mu}\Delta + V_L(\mathbf{r}), \tag{61}$$

where $V_L(\mathbf{r})$ is the interaction potential with a period L and μ is the reduced mass of the system. All the physical information is contained in the solutions of the stationary Schrödinger equation

$$H\psi = E\psi. \tag{62}$$

In the non-interacting region which we call Ω, the wave-function obeys the Helmholtz equation

$$(\Delta - k^2)\psi = 0, \tag{63}$$

where $E = k^2/2\mu$. Lüscher shows that there is a one-to-one correspondence between the periodic solutions of the Helmholtz equation with certain degree of singularity at the origin and the eigenfunctions of the Hamiltonian H [7] in the Ω region. In other words, once we have the solutions of Helmholtz equation, we can obtain the eigenfunctions of the Hamiltonian and then use them to compute the phase-shifts. The general singular periodic solution of the Helmholtz equation are

$$G(\mathbf{r}, k^2) = \sum_{l=0}^{\infty} \sum_{m=-l}^{l} v_{lm} G_{lm}(\mathbf{r}, k^2), \tag{64}$$

where v_{lm} are arbitrary coefficients and G_{lm} are the singular periodic solutions of the Helmholtz equation of degree l. We have

$$G_{lm}(\mathbf{r}; k^2) = \frac{(-)^l k^{l+1}}{4\pi} \left[Y_{lm}(\Omega) n_l(kr) + \sum_{l'm'} \mathscr{M}_{lm;l'm'} Y_{l'm'}(\Omega) j_{l'}(kr) \right], \tag{65}$$

where $Y_{lm}(\Omega)$ are the spherical harmonics, and $n_l(kr)$ and $j_l(kr)$ are the spherical Bessel functions of the first kind and second kind. The matrix $\mathscr{M}_{lm,l'm'}$ is given by

$$\mathscr{M}_{lm,js} = \frac{(-)^l}{\pi^{3/2}} \sum_{j=|l-l'|}^{l+l'} \sum_{s=-j}^{j} \frac{i^j}{q^{j+1}} Z_{js}(1; q^2) C_{lm,js,l'm'}, \tag{66}$$

where $C_{lm,js,l'm'}$ are related to the Wigner $3j$-symbols through

$$C_{lm,js,l'm'} = (-1)^{m'} i^{l-j+l'} \sqrt{(2l+1)(2j+1)(2l'+1)} \times \begin{pmatrix} l & j & l' \\ 0 & 0 & 0 \end{pmatrix} \begin{pmatrix} l & j & l' \\ m & s & -m' \end{pmatrix}. \tag{67}$$

The function $\mathscr{Z}$ is defined by

$$\mathscr{Z}_{lm}(s, q^2) = \sum_{\mathbf{n}} \frac{\mathscr{Y}_{lm}(\mathbf{n})^s}{n^2 - q^2}, \tag{68}$$

where $\mathscr{Y}_{lm}$ is the harmonic polynomials

$$\mathscr{Y}_{lm}(\mathbf{n}) = \mathbf{n}^l Y_{lm}(\Omega)\,. \tag{69}$$

On the other hand, we can obtain the eigenfunctions of the hamiltonian H using the spherical harmonics

$$\psi_{lm} = b_{lm}[\alpha_l(k)\, j_l(kr) + \beta_l(k) n_l(kr)], \tag{70}$$

for some constants b_{lm}. Because there is a one-to-one relation between the singular periodic solutions and eigenfunctions above, the matching between Eq. 65 and Eq. 70 becomes

$$\begin{aligned} b_{lm}\alpha_l(k) &= \sum_{l'=0}^{\infty}\sum_{m'=-l'}^{l'} v_{l'm'}\frac{(-)^{l'}k^{l'+1}}{4\pi}\mathscr{M}_{l'm';lm}, \\ b_{lm}\beta_l(k) &= v_{lm}\frac{(-)^{l}k^{l+1}}{4\pi}. \end{aligned} \tag{71}$$

The phase-shift is defined by the behavior of the wave-function in the free region and it is a function of the α and β coefficients:

$$e^{2i\delta_l(k)} = \frac{\alpha_l(k) + i\beta_l(k)}{\alpha_l(k) - i\beta_l(k)}. \tag{72}$$

Eq. 71 forms a homogeneous set of linear equations for coefficients b_{lm}. In order to have non-trivial solution for b_{lm}, it requires that

$$\det[e^{2i\delta} - U] = 0, \quad \text{where} \quad U = (\mathscr{M} + i)/(\mathscr{M} - i). \tag{73}$$

This is the general relation between the two-particle spectrum and the scattering phase-shifts and it holds even for relativistic systems up to exponentially small finite volume effects. In the relativistic case, one only needs to replace the non-relativistic energy momentum relation $E = k^2/2\mu$ with the relativistic form $W = 2\sqrt{m^2 + k^2}$.

In order to compute the $\mathscr{M}$ matrix, we introduce an orthonormal basis

$$|\Gamma, \alpha; l, n\rangle\,, \quad \alpha = 1, ..., \dim\Gamma \tag{74}$$

where Γ denotes one of the five irreps in cubic group, l denotes the infinte-volume representation of $SO(3)$ and n denotes the n-th occurance of the cubic irrp in the l representation. We compute the components of $\mathscr{M}$ in this basis. The Green function $G(\boldsymbol{r}; k^2)$ is invariant under cubic transformation and its derivatives transform as vectors. We have

$$G_{lm}(R\boldsymbol{r}; k^2) = \sum_{m'=-l}^{l} D^{(l)}_{mm'}(R) G_{lm'}(\boldsymbol{r}; k^2). \tag{75}$$

This leads to

$$\sum_{s=-l}^{l} D^{(l)}_{ms}(R)\mathscr{M}_{ls,l'm'} = \sum_{s'=-l'}^{l'} \mathscr{M}_{lm,l's'} D^{(l')}_{s'm'}(R). \tag{76}$$

If we consider the space of spherical harmonics up to degree $l \leq \Lambda$, the matrix $\mathscr{M}_{ls,l's'}$ can be viewed as an operator M in this space, and similarly the matrix inducing the rotations $D^{(l)}_{mm'}(R)$. The equation above implies that $\mathscr{M}$ and $D(R)$ commute for all R in the cubic group and thus a partial diagonalization of $\mathscr{M}$ can be achieved in a basis where D is diagonal, that is the irrep basis for the cubic group. This is the basis we constructed above. Using Schur's lemma [32], we can reduce the $\mathscr{M}$ matrix as

$$\langle \Gamma, \alpha; l, n\,|M|\,\Gamma', \alpha'; l'n'\rangle = \delta_{\Gamma\Gamma'}\delta_{\alpha\alpha'}\mathscr{M}(\Gamma)_{ln,l'n'}. \tag{77}$$

The values for the reduced $\mathscr{M}(\Gamma)$ are computed by Lüscher [7] for the cubic group and by Li [12] for the dihedral group.

C Quark Diagrams

In this subsection, we show the definition of the quarks diagrams used in calculation. The Γ structure are based on the rho interpolators we used in Table 3. For $C_{\rho_i \leftarrow \rho_j}$, we have

$$C_{\rho_i \leftarrow \rho_j} = -\left\langle \begin{array}{c} \Gamma^J_{t_f}, (\boldsymbol{p}, t_f) \\ \bigcirc \\ \Gamma^{J'\dagger}_{t_i}, (-\boldsymbol{p}, t_i) \end{array} \right\rangle = -\left\langle \mathrm{Tr}[M^{-1}(t_i, t_f)\Gamma^J_{t_f} e^{i\boldsymbol{p}} M^{-1}(t_f, t_i)\Gamma^{J'\dagger}_{t_i} e^{-i\boldsymbol{p}}] \right\rangle. \tag{78}$$

For $C_{\rho_i \leftarrow \pi\pi}$, we have a three-point diagram. The three vertices are filled by γ_5 and Γ^i. One can show that the disconnected quark diagrams will cancel after summing all the them in $I = 1$ channel due to isospin symmetry. The notation for the three-point quark diagrams is as follow:

$$\begin{array}{c} (\boldsymbol{p}_1 + \boldsymbol{p}_2, t_f) \\ \Gamma^i \\ \triangle \\ \gamma_5 \quad \gamma_5 \\ (-\boldsymbol{p}_1, t_i) \quad (-\boldsymbol{p}_2, t_i) \end{array} = \mathrm{Tr}[\tilde{M}(t_i, t_f)\Gamma^i_f e^{i(\boldsymbol{p}_1+\boldsymbol{p}_2)} \tilde{M}(t_f, t_i)\gamma_5 e^{-ip_2} \tilde{M}(t_i, t_i)\gamma_5 e^{-ip_1}]. \tag{79}$$

The correlation functions for $C_{\rho_i \leftarrow \pi\pi}$ are:

$$C_{\rho_i \leftarrow \pi\pi} = \left\langle \triangle - \triangle \right\rangle \overset{\boldsymbol{P}=0}{=} 2\left\langle \triangle \right\rangle. \tag{80}$$

Above we used the fact that when the total momentum $\boldsymbol{P}$ is zero, due to parity symmetry the clockwise and counter-clockwise diagrams have the same gauge filed average, that is

$$\left\langle \triangle \right\rangle = -\left\langle \triangle \right\rangle. \tag{81}$$

The correlation functions of $C_{\pi\pi \leftarrow \rho_i}$ are related to $C_{\rho_i \leftarrow \pi\pi}$ by doing the time reversal transform:

$$\left\langle \triangledown \right\rangle = \left\langle \triangle \right\rangle. \tag{82}$$

For $C_{\pi\pi \leftarrow \pi\pi}$, a number of diagrams cancel due to isospin symmetry. The diagrams that need to be evaluated are listed below

$$\begin{array}{cccc} (\mathbf{p_1}, t_f) \ (\mathbf{p_2}, t_f) & (\mathbf{p_1}, t_f) \ (\mathbf{p_2}, t_f) & (\mathbf{p_1}, t_f) \ (\mathbf{p_2}, t_f) & (\mathbf{p_1}, t_f) \ (\mathbf{p_2}, t_f) \\ \gamma_5 \ \gamma_5 & \gamma_5 \ \gamma_5 & \gamma_5 \ \gamma_5 & \gamma_5 \ \gamma_5 \\ \square & \bowtie & \text{⧓} & \bigcirc\!\bigcirc \\ \gamma_5 \ \gamma_5 & \gamma_5 \ \gamma_5 & \gamma_5 \ \gamma_5 & \gamma_5 \ \gamma_5 \\ (-\mathbf{p_1}, t_i) \ (-\mathbf{p_2}, t_i) & (-\mathbf{p_1}, t_i) \ (-\mathbf{p_2}, t_i) & (-\mathbf{p_1}, t_i) \ (-\mathbf{p_2}, t_i) & (-\mathbf{p_1}, t_i) \ (-\mathbf{p_2}, t_i) \end{array}. \tag{83}$$

The correlation function for $C_{\pi\pi\leftarrow\pi\pi}$ can be written as

$$C_{\pi\pi\leftarrow\pi\pi} = -\Big\langle$$ 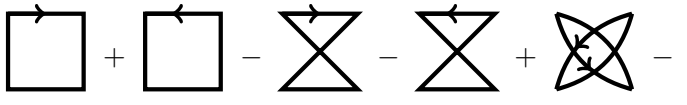 $$\Big\rangle . \qquad (84)$$

When the total momentum $\boldsymbol{P} = 0$, parity symmetry implies:

$$\Big\langle$$ 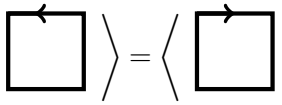 $$\Big\rangle = \Big\langle$$ 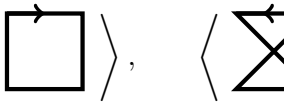 $$\Big\rangle , \qquad \Big\langle$$ 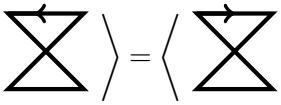 $$\Big\rangle = \Big\langle$$ $$\Big\rangle . \qquad (85)$$

Hence, the $C_{\pi\pi\leftarrow\pi\pi}$ correlation function is constructed from four four-point quark diagrams

$$C_{\pi\pi\leftarrow\pi\pi} = -\Big\langle 2$$ 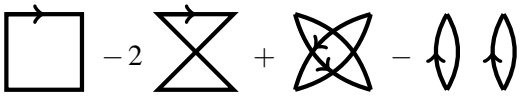 $$\Big\rangle . \qquad (86)$$

References

[1] C. McNeile and C. Michael (**UKQCD** Collaboration), *Phys.Lett.* **B556** (2003) 177–184, [hep-lat/0212020].

[2] S. Aoki *et. al.* (**CP-PACS** Collaboration), *Phys.Rev.* **D76** (2007) 094506, [arXiv:0708.3705].

[3] S. Aoki *et. al.* (**PACS-CS** Collaboration), *PoS* **LATTICE2010** (2010) 108, [arXiv:1011.1063].

[4] S. Aoki *et. al.* (**CS** Collaboration), *Phys.Rev.* **D84** (2011) 094505, [arXiv:1106.5365].

[5] K. Rummukainen and S. A. Gottlieb, *Nucl.Phys.* **B450** (1995) 397–436, [hep-lat/9503028].

[6] X. Feng, K. Jansen, and D. B. Renner, *Phys.Rev.* **D83** (2011) 094505, [arXiv:1011.5288].

[7] M. Luscher, *Nucl.Phys.* **B354** (1991) 531–578.

[8] M. Gockeler *et. al.* (**QCDSF** Collaboration), *PoS* **LATTICE2008** (2008) 136, [arXiv:0810.5337].

[9] M. Gockeler, R. Horsley, M. Lage, U.-G. Meissner, P. Rakow, *et. al.*, *Phys.Rev.* **D86** (2012) 094513, [arXiv:1206.4141].

[10] C. Lang, D. Mohler, S. Prelovsek, and M. Vidmar, *Phys.Rev.* **D84** (2011), no. 5 054503, [arXiv:1105.5636].

[11] C. Morningstar, J. Bulava, J. Foley, K. J. Juge, D. Lenkner, *et. al.*, *Phys.Rev.* **D83** (2011) 114505, [arXiv:1104.3870].

[12] X. Li and C. Liu, *Phys.Lett.* **B587** (2004) 100–104, [hep-lat/0311035].

[13] X. Feng, X. Li, and C. Liu, *Phys.Rev.* **D70** (2004) 014505, [hep-lat/0404001].

[14] C. Pelissier and A. Alexandru, *Phys.Rev.* **D87** (2013) 014503, [arXiv:1211.0092].

[15] A. Hasenfratz, R. Hoffmann, and S. Schaefer, *JHEP* **0705** (2007) 029, [hep-lat/0702028].

[16] J. J. Dudek, R. G. Edwards, and C. E. Thomas (**Hadron Spectrum** Collaboration), *Phys.Rev.* **D87** (2013), no. 3 034505, [arXiv:1212.0830].

[17] C. Lang, D. Mohler, S. Prelovsek, and M. Vidmar, *Phys.Rev.* **D84** (2011) 054503, [arXiv:1105.5636].

[18] C. Lang, L. Leskovec, D. Mohler, and S. Prelovsek, *Phys.Rev.* **D86** (2012) 054508, [arXiv:1207.3204].

[19] S. Prelovsek, L. Leskovec, C. Lang, and D. Mohler, *Phys.Rev.* **D88** (2013), no. 5 054508, [arXiv:1307.0736].

[20] Z. Fu and K. Fu, *Phys.Rev.* **D86** (2012) 094507, [arXiv:1209.0350].

[21] L. Maiani and M. Testa, *Phys.Lett.* **B245** (1990) 585–590.

[22] C. Gattringer and C. B. Lang, *Quantum Chromodynamics on the Lattice: An Introductory Presentation*. Springer, 2010.

[23] H. J. Rothe, *Lattice Gauge Theories: An Introduction, 4E*. World Scientific, 2012.

[24] M. Luscher and U. Wolff, *Nucl.Phys.* **B339** (1990) 222–252.

[25] B. Blossier, M. Della Morte, G. von Hippel, T. Mendes, and R. Sommer, *JHEP* **0904** (2009) 094, [arXiv:0902.1265].

[26] L. Maiani and M. Testa, *Phys.Lett.* **B245** (1990) 585–590.

[27] L. S. Brown and R. L. Goble, *Phys.Rev.Lett.* **20** (1968) 346–349.

[28] F. von Hippel and C. Quigg, *Phys. Rev. D* **5** (Feb, 1972) 624–638.

[29] J. J. Dudek, R. G. Edwards, and C. E. Thomas, *Phys.Rev.* **D86** (2012) 034031, [arXiv:1203.6041].

[30] J. Pelaez and G. Rios, *Phys.Rev.* **D82** (2010) 114002, [arXiv:1010.6008].

[31] C. Lang and V. Verduci, *Phys.Rev.* **D87** (2013), no. 5 054502, [arXiv:1212.5055].

[32] M. Hamermesh, *Group Theory and its Application to Physical Problems*. 1989.